
Extra-Cardiac Uptake of Technetium-99m-MIBI: Normal and Abnormal Variants

William W. Mohr, David L. Gibson and Willet Pang

Nuclear Medicine, Riverview Clinic-Dean Medical Center, Janesville, Wisconsin

Objective: Myocardial perfusion agents such as ^{201}Tl -chloride and $^{99\text{m}}\text{Tc}$ -sestamibi (Cardiolite, DuPont de Nemours, N. Billerica, MA) have been used with success in evaluating myocardial ischemia. Many authors have also found extracardiac uptake in the thorax for various pathological conditions when using both of these agents. This article explores both normal and abnormal variants of extracardiac uptake of $^{99\text{m}}\text{Tc}$ -sestamibi.

Methods: More than 400 consecutive patients from our lab were reviewed. We examined both normal and abnormal variants of extracardiac $^{99\text{m}}\text{Tc}$ -MIBI uptake in the thorax, and evaluated factors which may influence $^{99\text{m}}\text{Tc}$ -sestamibi uptake.

Results: This paper describes cases of previously undiagnosed broncho-alveolar carcinoma and thymoma. Possible explanations for $^{99\text{m}}\text{Tc}$ -MIBI uptake in other extracardiac sites are presented, including the sternum, thoracic spine and thyroid.

Conclusion: A series of coronal slices may prove useful in all myocardial perfusion studies. This can be accomplished with only incidental institutional cost. The additional information can aid in early diagnosis of unknown thoracic pathologies which physiologically incorporate this agent.

Key Words: technetium-99m-MIBI; normal variants; cardiac imaging; extracardiac uptake

J Nucl Med Technol 1996; 24:104-111

Technetium-99m-methoxyisobutyl isonitrile (MIBI) has been primarily used to evaluate myocardial ischemia. Additional investigation has found that this agent also successfully localizes in parathyroid adenomas (1,2), undifferentiated mesenchymal tumors (3), malignant and benign bone lesions (4,5), thyroid cancer and its metastases (6-9), esophageal carcinoma (10), lung carcinomas (11,12), sarcoidosis (13), ACTH-producing tumors (14) and breast carcinoma (15-17). Many of these sites of abnormal extracardiac uptake appear within the standard field-of-view for myocardial perfusion imaging.

For correspondence or reprints contact: William W. Mohr, MBA, CNMT, Nuclear Medicine, Riverview Clinic-Dean Medical Ctr., P.O. Box 551, 580 North Washington, Janesville, WI 53547-0551.

MATERIALS AND METHODS

We evaluated 478 patients for myocardial ischemia using $^{99\text{m}}\text{Tc}$ -sestamibi from July 1994 until May 1995. After an initial resting study in which 8-10 mCi of MIBI was injected, a stress study was done at least 4 hr later.

For stress imaging, 25-30 mCi of $^{99\text{m}}\text{Tc}$ -MIBI were injected at peak exercise or 4 min post-intravenous dipyridamole (intravenous Persantine, DuPont de Nemours, N. Billerica, MA) infusion. At 30-60 min postinjection, a 180° SPECT dataset was acquired from 45° RAO to 45° LPO using a single-head scintillation detector (PRISM, Picker International, Cleveland, OH) with a high-resolution hexagonal parallel-hole collimator. Sixty images were acquired for 15 and 20 sec at stress and rest, respectively; each using a 140-keV photopeak with a 15% window.

Prior to processing, the stress and rest data sets were first evaluated for motion by observing a cine of the raw data. Once motion was determined to be nonexistent, each image set was prefiltered with a low-pass filter with an order of 5.0 and a cut-off frequency adjusted to reduce the noise component to 10%. Transaxial slices were then reconstructed using a Ramp filter and were reformatted to create coronal slices each with a thicknesses of 1.2 cm. Attenuation correction was not used in this process. The stress (and rest in some cases) coronal slices were displayed on a blue base infrared laser imaging film with the maximum pixel value set at 40% of the true top pixel value, thereby increasing image contrast in the lower count range of the images. If an area of uptake appeared suspicious, a rotating three-dimensional volume-rendered image set (Max Pixel Ray-trace software, Picker International, Cleveland, OH) was viewed on the console using the same windowing as that used for displaying coronal slices. Additional aids in evaluating suspicious uptake were sagittal slices of both the stress and rest data, chest x-rays, CT scans of the ROI, and/or cine review of the raw data.

Evaluation of what we believe to be red bone marrow uptake in the sternum and the spine was performed on two separate groups of 20 patients. One group was undergoing rest/persantine testing and the second group was undergoing rest/exercise testing. Using sagittal slices of 1.2 cm, a separate ROI was

TABLE 1
Technetium-99m-Sestamibi Visible Extracardiac Uptake By Site (n = 478)

Area of sestamibi uptake	Number of patients	Percent of patients
Right deltoid/triceps	418	87.5
Left latissimus dorsi	416	87.0
Thyroid gland	202	42.2
Sternum	122	25.5
Global lung uptake	106	22.2
Ribs	93	19.5
Thoracic spine	88	18.4
Right pectoralis major	15	3.1
Elevated liver	7	1.5
Right sternocleidomastoid	5	1.0
Salivary glands	3	0.6
Hiatal hernia	2	0.4
Focal lung uptake	2	0.4
Arm injection tract	1	0.2

drawn around the sternum and spine at rest and stress in each group. The mean counts per pixel within this ROI was then used in the evaluation. Stress counts were corrected for physical decay of the rest dose, and differences in both dose and acquisition times per frame for rest and stress exams. It was assumed that there was negligible washout of ^{99m}Tc-MIBI from the site of accumulation (red bone marrow).

RESULTS

Extracardiac areas of observed MIBI uptake in this patient population are listed in order of frequency in Table 1. Of the 418 patients with right deltoid/tricep uptake and 416 with left latissimus dorsi uptake, 390 patients had visual uptake in both areas (Fig. 1). Skeletal uptake occurred in the sternum, spine and ribs (Fig. 2). Of the patients who had skeletal uptake, uptake occurred in two areas 56% of the time and all three areas 29% of the time.

Technetium-99m-sestamibi, when compared to ²⁰¹Tl, has a greater amount of lung uptake at 60 mins (18). Therefore, it was not surprising that ^{99m}Tc-sestamibi lung uptake was present in a notable number of patients. Global lung uptake of ^{99m}Tc-MIBI was defined as one or both lung fields having elevated uniform uptake. The lung-to-heart ratios were evaluated to determine if the method of displaying the image on film

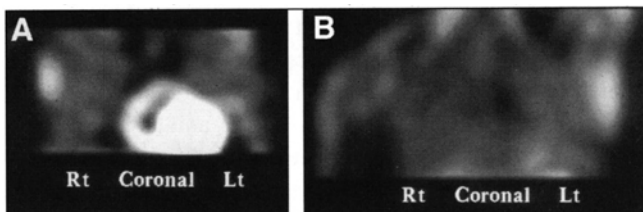


FIGURE 1. (A) Coronal slice displaying right pectoralis major in addition to the right and left ventricles of the heart. (B) Mid-thoracic coronal slice showing right deltoid-tricep, sternocleidomastoids, and left latissimus dorsi.

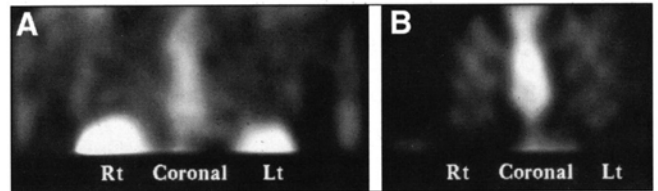


FIGURE 2. (A) Posterior thoracic coronal slice through the thoracic spine; also present are the liver and spleen. (B) Anterior thoracic coronal slice showing the ribs and sternum.

affected global lung visualization. Lung-to-heart ratios were evaluated in 30 consecutive patients in which global lung uptake was observed and an additional 30 patients in which it went unobserved. This was done by placing a 3 × 3-pixel ROI over a region in the lung and left ventricular myocardium on the same coronal slice. Patients in which global lung uptake went unobserved had a mean lung-to-heart ratio of 13% with a range of 4–19% while those patients determined to have global lung uptake had an average lung-to-heart ratio of 23% with a range of 14–38%.

Focal lung uptake was defined as an area or areas in the lung where ^{99m}Tc-MIBI accumulation was elevated but the surrounding lung tissue uptake was uniformly lower. Two patients, both presenting with chest pain, fit this criteria. In one case, retrosternal uptake was seen with the lesion-to-heart ratio found to be 43%. Bronchoalveolar cancer was ultimately diagnosed. Focal uptake in the anterior right mediastinum was seen in the second case. The lesion-to-heart ratio for this area was found to be 28%. A benign thymoma was later diagnosed. For both patients, different coronal slices were used for the heart and lesion ROI due to the location where each was observed.

A significant portion of this study was dedicated to evaluating skeletal ^{99m}Tc-MIBI uptake and to determining if intravenous dipyridamole, state of exercise (rest or stress) and history of sternotomy influenced this uptake. Table 2 is a summary of the observed uptake sites in the entire population classified as to the type of stress procedure done. Twenty patients from each group were then randomly selected and evaluated. Irregular ROIs were placed around the spine and sternum at both rest and stress. Coronal image sets at rest for both groups were also created and displayed on film. The data from this evaluation is listed in Table 3. The average maximum pixel value for each group is listed because of the method in which the coronal slices were displayed: 40% of the maximum pixel value. It

TABLE 2
Technetium-99m-Sestamibi Visual Uptake by Site

	Intravenous persantine	Exercise stress
Number of patients	102	376
Sternum	75 (74%)	47 (13%)
Thoracic spine	68 (67%)	20 (5%)
Ribs	36 (35%)	57 (15%)

TABLE 3
Uptake of Sestamibi with Different Types of Stress*

	Intravenous persantine	Exercise	T-test
Number of Patients	20	20	
Sternum visualization	Rest: 15 Stress: 17	Rest: 15 Stress: 3	
Spine visualization	15	0	
Body surface area	Mean = 1.91	Mean = 1.93	
Corrected sternal uptake stress/rest	Mean = 1.44 s.d. = 0.54	Mean = 0.71 s.d. = 0.31	t = 5.3 p < 0.001
Average maximum pixel value at stress	1782	2302	

*No patient in this group had ever undergone sternotomy

should be noted that a 29% increase in maximum pixel value in the exercise stress image is at least partly responsible for the lack of marrow visualization in this group.

Table 4 was derived from the International Commission on Radiological Protection reference data to illustrate the percentage of red bone marrow by weight at various thoracic sites and was used to evaluate if the location of red bone marrow had an effect on site visualization (19). How these values were attained can be illustrated by the following example of the sternum:

Relative percent of dry bone weight in an adult = 0.65%
 Total bone weight (g) in a skeleton (dry or undry unknown) = 5000 g
 Sternum weight (bone only): $0.0065 \times 5000 = 32.5$ g
 Total marrow weight (red and yellow): 39 g
 Red marrow weight: 23.4 g
 Weight percent of red marrow:

$$\frac{23.4}{(39 + 32.5)} \times 100 = 32.7\%$$

DISCUSSION

The uptake and concentration of ^{99m}Tc -MIBI is directly related to regional blood flow (20), elevated cell membrane

TABLE 4
Red Bone Marrow Evaluation

Site	Total weight (g) without marrow	Total marrow weight (g)	Red marrow weight (g)	Red marrow percent weight of site
Scapula	78.0	33.7	25.2	22.6
Clavicle	27.0	10.8	8.1	21.4
Sternum	32.5	39.0	23.4	32.7
Ribs (3-8) average	27.7	30.0	8.7	15.1
Thoracic vertebrae (3-8) average	18.2	14.5	10.9	33.3

potentials (21,22), cell (23) and mitochondrial viabilities (24), and the mitochondrial density (25). Therefore, sestamibi does not have the same mechanism of uptake as ^{201}Tl -chloride which is taken up as a potassium analog. All of these factors must be taken into consideration when evaluating the following areas of observed extracardiac ^{99m}Tc -MIBI uptake.

Musculoskeletal Tissue Uptake

The skeleton is composed of compact and cancellous bone. Compact bone is chiefly responsible for maintaining the structure of the body, but also plays a part in calcium regulation and osteogenesis in both youth and when skeletal integrity has been compromised. Cancellous bone is composed of interconnected trabeculae and is the site of both red and yellow bone marrow, each of which are seen in nearly equal amounts in the adult (26). The yellow marrow is primarily fat and is located in the shafts of long bones. It serves little function other than providing additional support to the bones in which it is located. In some pathological situations, however, yellow marrow can convert to red marrow. The red marrow is largely responsible for hematopoiesis and receives a blood supply that is 90% of that which is received by the liver (27). Red marrow blood flow has been found to be significantly greater than blood flow in the cortical bone except in growing metaphyseal regions or in areas where vascular enhancement results from some skeletal tumors or localized cortical inflammations (28,29). As an individual ages, however, red marrow blood flow decreases due to a fall in the number of both osteoclast and hemopoietic cells within the marrow (30). In the normal adult, red marrow is located in the skull, vertebral bodies, flat bones, ends of long bones, and some short bones. Of these sites, the sternum, thoracic spine and ribs were evaluated for uptake of ^{99m}Tc -MIBI rather than the humeral head and neck, clavicular ends and scapulae. The red marrow in these latter three sites is located at the bone ends, thereby making it difficult to be included in the camera field of view and/or is near musculoskeletal tissue, thus making differential uptake difficult to consistently separate from surrounding tissue.

We believe the site of ^{99m}Tc -MIBI uptake in the skeleton is the red bone marrow based on little or no ^{99m}Tc -MIBI uptake being visually present on coronal slices of areas free of red marrow such as the humeral shaft. Technetium-99m-MIBI uptake was commonly seen in red marrow areas of the sternum, ribs and thoracic spine (Fig. 3). Little to no ^{99m}Tc -MIBI was seen in red marrow-free regions, even when bone turnover rates are elevated due to recent fracture. In seven patients recently experiencing traumatic fractures to cortical bone sites, Caner, et al. (4) found no differential uptake of ^{99m}Tc -MIBI at the fracture sites when compared to the uninjured contralateral site. Without performing bone marrow biopsies, the above observations appear to be the most likely explanation for determining the skeletal compartment in which ^{99m}Tc -MIBI localizes.

In our study population of 478 patients, ^{99m}Tc -MIBI uptake was seen on stress coronal slices in the sternum (25.5%), ribs

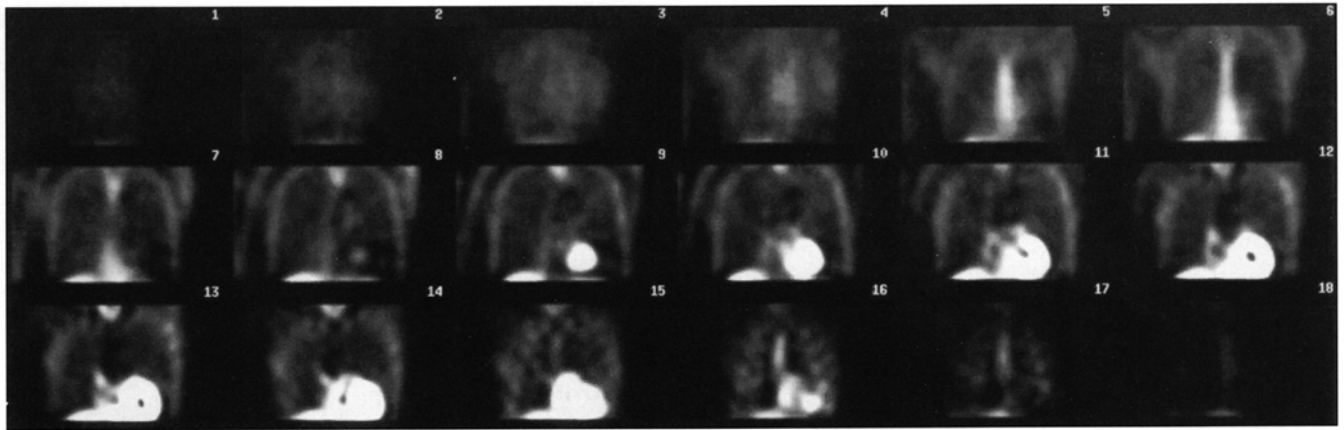


FIGURE 3. Standard coronal slices posterior to anterior showing significant amount of bone marrow uptake. The auricle of the right atrium has focal uptake of ^{99m}Tc -MIBI giving the appearance of extracardiac uptake.

(19.5%) and thoracic spine (18.4%). When comparing pharmacological stress to exercise stress, we observed sternal, thoracic spine and rib uptake more often when intravenous persantine was used. However, when looking at sternal visualization at rest in a subgroup of 40 sternotomy-free patients undergoing either intravenous persantine or stress myocardial perfusion imaging, there was no difference between either group.

These differences in visualization were likely due to changes in the percentage of cardiac output to different systems during maximum stress. It has been previously calculated that cardiac output to the musculoskeletal system is 20% at rest versus 88% at maximum stress (31). Gross, et al. (32) found that during exercise, vascular resistance in the bone marrow increased two- to fourfold but fell significantly in musculoskeletal tissue. At stress, the uptake of ^{99m}Tc -MIBI (measured as the mean counts per pixel) in the sternum and thoracic spine fell by 42% and 31%, respectively, in this investigation.

Gross, et al. (32) also found that vasoactive drugs, such as adenosine, decreased vascular resistance in the bone marrow. When using intravenous persantine, ^{99m}Tc -MIBI uptake (measured as counts per pixel) was found to increase in the sternum and thoracic spine by 44% and 24%, respectively, with a significant difference in ^{99m}Tc -MIBI uptake in both areas between the two groups when evaluated with a two-tailed t-test ($p < 0.001$). Due to minimal differences in body surface areas between the two groups, it is suspected that the difference in

^{99m}Tc -MIBI uptake between the spine and sternum is influenced by both differential attenuation and variations in detector-to-source distances between the sites.

Bone marrow visualization on film is at least partly influenced by the maximum pixel count from which the image is scaled and must be taken into consideration. The average maximum pixel count in the intravenous persantine group was 1,782 compared to 2,302 in the exercise stress group; a 29% difference. When scaling to 40% of the maximum pixel, a higher maximum pixel value will make it more difficult to see areas of low to moderate ^{99m}Tc -MIBI uptake due to lower image contrast.

Lee, et al. (33) theorized that sternal visualization in a patient undergoing an adenosine myocardial perfusion scan with ^{99m}Tc -MIBI was likely due to a sternotomy 10 days prior to the exam. Two groups of patients were evaluated to determine if sternotomy influenced ^{99m}Tc -MIBI uptake. The results are listed in Table 5. One group of 4 patients had two previous imaging procedures; one prior to sternotomy and the second shortly afterwards (mean time = 3 mo). In the second group, 6 patients with previous sternotomies (mean time = 27 mo) were compared with 6 patients who had never undergone sternotomy. Sternal uptake at rest was 47% greater in the first group of patients, while no difference between rest and stress uptake is found in the second group of patients. This suggests that the sooner an exam was done post-sternotomy, the greater the uptake of ^{99m}Tc -MIBI uptake in the sternum.

TABLE 5
Sternal Uptake of Technetium-99m-Sestamibi

	Group 1 (N = 4)		Group 2 (N = 6)	
	Pre-CABG	Post-CABG	Pre-CABG	Post-CABG
Months post-CABG	N/A	3.0	N/A	27
Visualization at rest	3 of 4 = 75%	4 of 4 = 100%	3 of 6 = 50%	4 of 6 = 67%
Visualization at stress	0 of 4 = 0%	1 of 4 = 25%	0 of 6 = 0%	0 of 6 = 0%
Corrected sternum counts = stress/rest	0.41	0.56	0.60	0.40
Sternal counts at rest	78	115	79	77

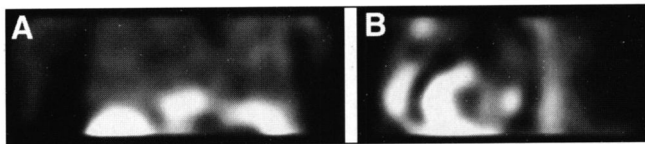


FIGURE 4. (A) Posterior thoracic coronal slice of the liver, hiatal hernia and spleen. (B) Sagittal slice of hiatal hernia posterior to the myocardium.

In conclusion, resting states at injection and intravenous dipyridamole infusion both have a direct effect on ^{99m}Tc -MIBI uptake in the bone marrow. Due to a small population size, we were unable to determine if recent sternotomy also directly influences ^{99m}Tc -MIBI uptake. It should be noted, however, that an attempt to differentiate degrees of uptake or subdivide uptake levels into normal and abnormal groups was not made. Myelodysplastic disease has already been shown to be associated with elevated ^{99m}Tc -MIBI uptake in the sternum (34), but additional research is necessary to determine if the level of ^{99m}Tc -MIBI uptake is relevant to other pathological conditions of the red marrow.

Hepatobiliary System Uptake

The most significant route for ^{99m}Tc -MIBI elimination from the body is through the hepatobiliary system. Within 48 hr of a rest injection of ^{99m}Tc -MIBI, 36.9% is excreted in the feces (20). This figure drops to 29.1% if injection occurs at stress. Duodenal reflux of hepatobiliary agents into the stomach has been observed as a sign of acute cholecystitis (35) and significant duodenal pathology (36). The reflux of ^{99m}Tc -MIBI into the stomach and esophagus has also been documented (37,38).

In our group of patients, two cases were observed where both gastro-duodenal reflux into a hiatal hernia (Figs. 4, 5) occurred rendering the stomach visible posterior to the heart.

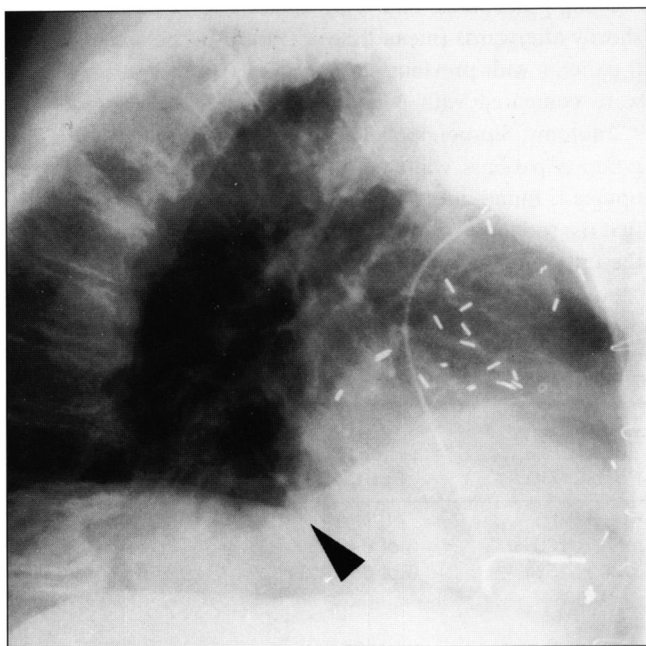


FIGURE 5. Lateral chest x-ray of a hiatal hernia (arrow).

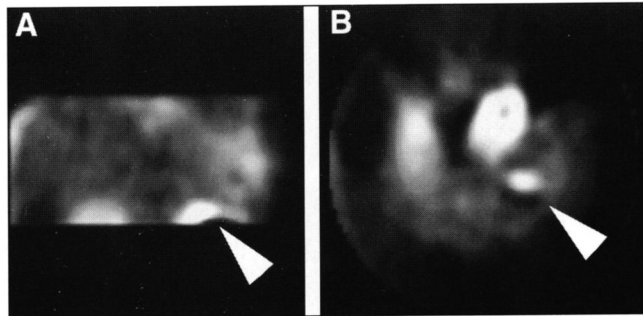


FIGURE 6. (A) Posterior thoracic coronal slice of an elevated loop of small bowel. (B) Transaxial slice of elevated loop of small bowel posterior to the myocardium.

A hiatal hernia occurs when a portion of the abdominal viscera, usually the gastric cardia of the stomach, ascends into the thorax through the esophageal opening in the diaphragm. Depending on the severity of the hernia, a significant portion of the stomach could ascend posterior to the heart. In a third patient, significant diaphragmatic reconstruction resulted in small bowel visualization much superior to what is normally seen (Figs. 6, 7). Therefore, when ^{99m}Tc -MIBI uptake occurs in the inferior portion of the thorax, either retrocardiac or at the same level to the myocardium, careful examination for a hiatal hernia or small bowel should be considered.

Thyroid Uptake

As observed in parathyroid imaging, significant uptake but differential washout of ^{99m}Tc -MIBI by the thyroid and parathyroid adenomas necessitates delayed imaging to localized retrothyroid parathyroid adenomas (1). Savi, et al. (39) found that the thyroid was the critical organ when ^{99m}Tc -MIBI was injected at rest. They theorized that ^{99m}Tc -MIBI was degraded to ^{99m}Tc -pertechnetate in-vivo. Although a small amount

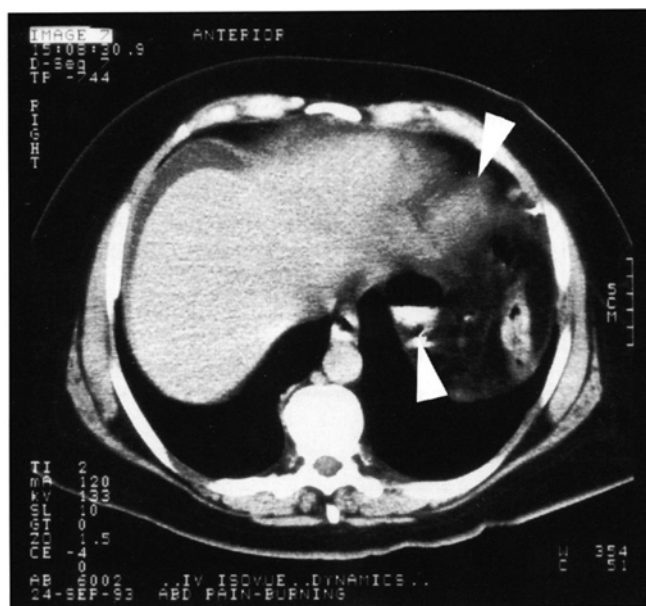


FIGURE 7. CT transaxial of loop of small bowel (arrows to myocardium and small bowel loop)

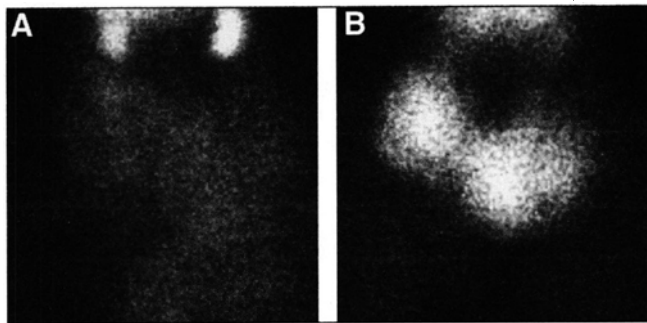


FIGURE 8. (A) Thyroid scan of a patient on synthroid using ^{99m}Tc -pertechnetate. (B) Thyroid scan of the same patient using ^{99m}Tc -sestamibi. Imaging times were equal for each.

of free pertechnetate may contribute to thyroid visualization, the thyroid has been shown to accumulate ^{99m}Tc -MIBI even when it was suppressed with perchlorate (40). Autonomous functioning thyroid nodules also may accumulate ^{99m}Tc -MIBI (41,42). In an additional investigation into the uptake mechanisms of ^{99m}Tc -MIBI in the thyroid, Folde, et al., (43) evaluated thyroid imaging with both ^{99m}Tc -pertechnetate and ^{99m}Tc -MIBI in 58 patients. In 34 patients, in whom a cold nodule was seen with ^{99m}Tc -pertechnetate, histopathological evaluation revealed a low correlation between ^{99m}Tc -MIBI uptake and malignancy. They did determine, however, the maximum uptake of ^{99m}Tc -MIBI in the thyroid was at 4 min and the half-time clearance was at 27 min postinjection.

In order to determine if noninclusion of the thyroid within the imaging field of view was the main reason for thyroid nonvisualization in 58% of the patients in this study group, 21 consecutive patients were specifically evaluated for thyroid uptake. A 3-min planar image of the neck was acquired at approximately 1.5 hr postinjection of the stress dose. All 21 images demonstrated at least faint visualization of the thyroid, as well as salivary gland and sternocleidomastoid uptake, with a normalized mean thyroid-to-background ratio equal to 1.4.

It is likely that the thyroid will be present on a coronal series if it is included in the field of view during acquisition because SPECT reconstruction increases image contrast. It is also evident from the results of other authors that the intensity of thyroid visualization is at least partly related to the time at which acquisition is obtained after injection. Although an attempt to correlate ^{99m}Tc -MIBI uptake with thyroid function was not made in this study, some researchers have found that significantly greater uptake occurs in patients with hyperthyroidism compared to those who are euthyroid (44). It should also be emphasized that thyroid uptake can be expected to occur, even when thyroid function is pharmacologically or pathologically suppressed (Fig. 8).

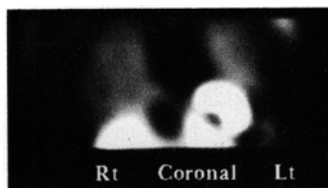


FIGURE 9. Mid-thoracic coronal slice demonstrating global lung uptake.

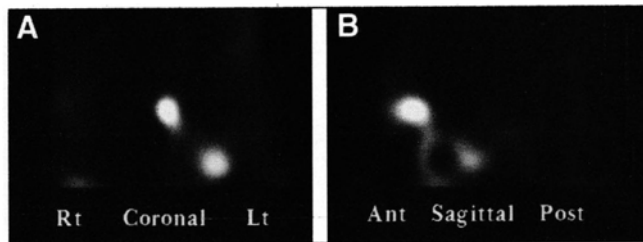


FIGURE 10. (A) Anterior thoracic coronal slice of a retrosternal bronchioalveolar CA. (B) Sagittal slice of the same patient.

Global Lung Uptake

Lung-to-heart ratios of ^{99m}Tc -sestamibi uptake at 30–60 min postinjection were evaluated by Giubbini, et al., (18) to determine if they were a reliable predictor of left ventricular function. When ratios were greater than 0.47, over 68% of the patients evaluated had a left ventricular ejection fraction less than 40%. Giubbini also theorized that the delay in washout of ^{99m}Tc -sestamibi from the lungs when compared to ^{201}Tl -chloride was due to a difference in the uptake mechanisms of each radiopharmaceutical. Although an attempt to correlate lung uptake to any specific measure of myocardial function was not made in this study, markedly elevated bilateral global lung uptake may prove to be a likely indicator of left ventricular dysfunction (Fig. 9).

Focal Lung Uptake

Many malignant tumors exhibit higher metabolic rates with greater negative cell transmembrane potentials to meet these metabolic needs. This would account for an increased accumulation of ^{99m}Tc -MIBI when compared to normal surrounding tissues. In the study sample, one patient with increased ^{99m}Tc -MIBI uptake had an undiagnosed retro-sternal malignant bronchioalveolar cancer (Figs. 10, 11). Another patient had an undiagnosed benign thymoma (Figs. 12, 13). The lesion-to-heart ratios were 43% and 28%; the lesion-to-normal lung tissue ratios were 4.7 and 2.2. Although the number of patients

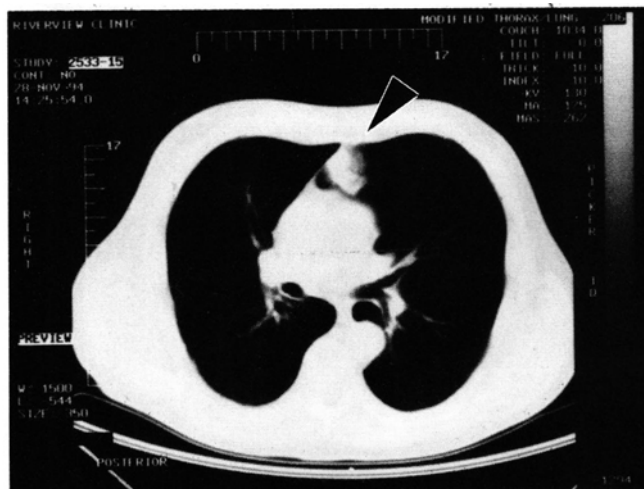


FIGURE 11. Transaxial CT image of the same patient showing the tumor (arrow).

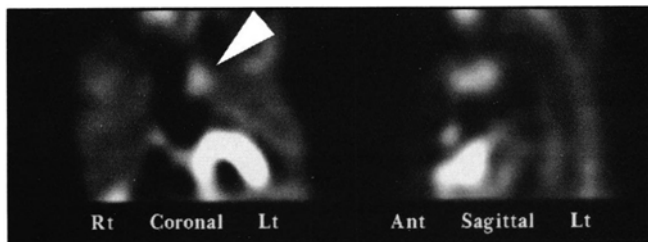


FIGURE 12. (A) Mid-thoracic coronal slice of a thymoma. (B) Sagittal slice of the same patient.

displaying focal lung uptake was small in our study, our observations of the lung agree with those of Caner, et al. (4). Technetium-99m-MIBI uptake was greater in malignant lesions compared to benign lesions.

Breast Uptake

Breast uptake of ^{99m}Tc -MIBI was not observed in this study group. Breast malignancies and accompanying lymphadenopathy could be in the camera field of view during myocardial perfusion imaging.

If ^{99m}Tc -MIBI activity greater than background is observed anterior to the thoracic wall, and/or focal activity in an auxiliary lymph node is unaccompanied by dose infiltration of the affected side, further investigation into the possibility of breast malignancy may be called for.

CONCLUSION

This study evaluated the frequency of both clinically significant and clinically nonsignificant extracardiac uptake of ^{99m}Tc -MIBI when using coronal slices of the thorax obtained from myocardial perfusion SPECT data. An explanation based on observation and a literature review for the mechanisms



FIGURE 13. Transaxial CT image of the same patient showing the thymoma (arrow).

responsible for extracardiac uptake in each specific group of observations was presented.

The incidence of clinically significant ^{99m}Tc -MIBI extracardiac uptake was low (0.42%) in our patient population. Further studies should be carried out in each department to determine if generation of full field-of-view SPECT reconstruction (transaxial, coronal and/or sagittal slices) warrants inclusion in review and/or display protocols for ^{99m}Tc -MIBI myocardial perfusion data.

REFERENCES

1. Taillefer R, Boucher Y, Potvin C, et al. Detection and localization of parathyroid adenomas in patients with hyperparathyroidism using a single radionuclide imaging procedure with technetium-99m-sestamibi (double-phase study). *J Nucl Med* 1992;33:1807-1809.
2. O'Doherty MJ, Kettle AG, Wells P, et al. Parathyroid imaging with technetium-99m-sestamibi: preoperative localization and tissue uptake studies. *J Nucl Med* 1992;33:313-318.
3. Caner B, Kitapci M, Erben G, et al. increased accumulation of ^{99m}Tc -MIBI in undifferentiated mesenchymal tumor and its metastatic lung lesions. *Clin Nucl Med* 1992;17:144-145.
4. Caner B, Kitapci M, Unlu M, et al. Technetium-99m-MIBI uptake in benign and malignant bone lesions: a comparative study with technetium-99m-MDP. *J Nucl Med* 1992;33:319-324.
5. Caner B, Kitapci M, Aras T, et al. Increased accumulation of hexakis (2-methoxyisobutylisonitrile) technetium(I) in osteosarcoma and its metastatic lymph nodes. *J Nucl Med* 1991;32:1977-1978.
6. Balon HR, Fink-Bennett D, Stoffer SS. Technetium-99m-sestamibi uptake by recurrent hurthle cell carcinoma of the thyroid. *J Nucl Med* 1992;33:1393-1395.
7. Scott AM, Kostakoglu L, O'Brien JP, et al. Comparison of technetium-99m-MIBI and thallium-201-chloride uptake in primary thyroid lymphoma. *J Nucl Med* 1992;33:1396-1398.
8. O'Driscoll CM, Baker F, Casey MJ, et al. Localization of recurrent medullary thyroid carcinoma with technetium-99m-methoxyisobutylisonitrile scintigraphy: a case report. *J Nucl Med* 1991;32:2281-2283.
9. Yen TC, Lin HD, Lee CH, et al. The role of technetium-99m sestamibi whole-body scans in diagnosing metastatic hurthle cell carcinoma of the thyroid gland after total thyroidectomy: a comparison with iodine-131 and thallium-201 whole body scans. *Eur J Nucl Med* 1994;21:980-983.
10. Kao CH, Wang SJ, Chen CY, et al. Detection of esophageal carcinoma using ^{99m}Tc -MIBI SPECT imaging. *Clin Nucl Med* 1994;19:1069-1074.
11. Abdel-Dayem HM, Scott A, Macapinlac H, et al. Tracer imaging in lung cancer. *Eur J Nucl Med* 1994;21:57-81.
12. Hassan IM, Sahweil A, Constantinides C, et al. Uptake and kinetics of Tc-99m hexakis 2-methoxy isobutyl isonitrile in benign and malignant lesions in the lungs. *Clin Nucl Med* 1989;14:333-340.
13. Aktulun C, Bayhan H. Tc-99m MIBI uptake in pulmonary sarcoidosis: preliminary clinical results and comparison with Ga-67. *Clin Nucl Med* 1994;19:1063-1065.
14. Jacobsson H, Wallin G, Werner S, et al. Technetium-99m methoxyisobutylisonitrile localizes an ectopic ACTH-producing tumour: case report and review of the literature. *Eur J Nucl Med* 1994;21:582-586.
15. Campeau RJ, Kronemer KA, Sutherland CM. Concordant uptake of Tc-99m sestamibi and Tl-201 in unsuspected breast tumor. *Clin Nucl Med* 1992;17:936-937.
16. Scopinaro F, Schillaci O, Scarpini M, et al. Technetium-99m sestamibi: an indicator of breast cancer invasiveness. *Eur J Nucl Med* 1994;21:984-987.
17. Khalkhali I, Mena I, Diggles L. Review of imaging techniques for the diagnosis of breast cancer: a new role of prone scintimammography using technetium-99m sestamibi. *Eur J Nucl Med* 1994;21:357-362.
18. Giubbini R, Campini R, Milan E, et al. Evaluation of technetium-99m-sestamibi lung uptake: correlation with left ventricular function. *J Nucl Med* 1995;36:58-63.
19. International Commission on Radiological Protection. Report of the task

- group on reference man. Publication number 23. New York, NY: Pergamon Press; 1975: data from tables 14 and 31.
20. Wackers FJ, Berman DS, Maddahi J, et al. Technetium-99m hexakis 2-methoxyisobutyl isonitrile: human biodistribution, dosimetry, safety, and preliminary comparison to thallium-201 for myocardial perfusion imaging. *J Nucl Med* 1989;30:301-311.
 21. Delmon-Moingeon LI, Piwnica-Worms D, Van den Abbeele AD, et al. Uptake of the cation hexakis (2-methoxyisobutylisonitrile)-technetium-99m by human carcinoma cell lines in vitro. *Cancer Research* 1990;50:2198-2202.
 22. Piwnica-Worms D, Kronauge JF, Chiu ML. Enhancement by tetraphenylborate of technetium-99m-MIBI uptake kinetics and accumulation in cultured chick myocardial cells. *J Nucl Med* 1991;32:1992-1999.
 23. Beanlands RS, Dawood F, Wen WH, et al. Are the kinetics of technetium-99m methoxyisobutyl isonitrile affected by cell metabolism and viability? *Circulation* 1990;82:1802-1814.
 24. Crane P, Laliberte R, Heminway S, et al. Effect of mitochondrial viability and metabolism on technetium-99m-sestamibi myocardial retention. *Eur J Nucl Med* 1993;20:20-25.
 25. Piwnica-Worms D, Holman BL. Noncardiac applications of hexakis (Alkylisonitrile) technetium-99m complexes. *J Nucl Med* 1990;31:1166-1167.
 26. Bonner H. The blood and the lymphoid organs. In: Rubin E, Faber JL, eds. *Pathology*. Philadelphia, PA: Lippincott; 1988:104.
 27. Collier DB, Sodee BD, Robinson RG. Bone. In: Murray IPC, Ell PJ, eds. *Nuclear medicine in clinical diagnosis and treatment, Volume 2*. New York, NY: Churchill Livingstone; 1994:339-334.
 28. Tondevold E, Eliassen P. Blood flow rates in canine cortical and cancellous bone measured with ^{99m}Tc-labeled albumin microspheres. *ACTA Ortho Scand* 1982;53:7-11.
 29. Brookes M. Blood flow rates in compact and cancellous bone, and bone marrow. *J of Anat* 1967;101:533-541.
 30. Kita K, Kawai K, Hirohata K. Changes in bone marrow blood flow with aging. *J Ortho Res* 1987;5:569-575.
 31. McArdle WD, Katch FI, Katch VL. *Exercise physiology: energy, nutrition, and human performance*, 2nd ed. Malvern, PA: Lea and Febiger 1991:334-335.
 32. Gross PM, Heistad DD, Marcus ML. Neurohumoral regulation of blood flow to bones and marrow. *Am J of Phys* 1979;237(4):440-448.
 33. Lee JD, Kim SM, Park CH. Technetium-99m-MIBI uptake in the sternum. *Clin Nucl Med* 1992;17:819.
 34. Thomas PA, Gibbons RJ. Technetium-99m-sestamibi marrow uptake in a patient with myelodysplastic syndrome. *Clin Nucl Med* 1994;19:617-618.
 35. Colletti PM, Barakos JA, Siegel ME, et al. Enterogastric reflux in suspected acute cholecystitis. *Clin Nucl Med* 1987;12:533-535.
 36. Drane WE, Hanner JS. Complete duodenogastric reflux: a scintigraphic sign of significant duodenal pathology. *J Nucl Med* 1989;30:1568-1570.
 37. Middleton GW, Williams JH. Significant gastric reflux of technetium-99m-MIBI in SPECT myocardial imaging. *J Nucl Med* 1994;35:619-620.
 38. Travin MI, Demus DD, Grant N, et al. First impressions: reflux esophagitis as the cause of atypical chest pain. *J Nucl Med* 1994;35:637.
 39. Savi A, Gerundini P, Zoli P, et al. Biodistribution of Tc-99m-methoxyisobutyl-isonitrile (MIBI) in humans. *Eur J Nucl Med* 1989;15:597-600.
 40. Civelek AC, Durski K, Shafique I, et al. Failure of perchlorate to inhibit Tc-99m isonitrile binding by the thyroid during myocardial perfusion studies. *Clin Nucl Med* 1991;16:358-361.
 41. Ramanathan P, Patel RB, Subrahmanyam N, et al. Visualization of suppressed thyroid tissue by technetium-99m-tertiary butyl isonitrile: an alternative to post-TSH stimulation scanning. *J Nucl Med* 1990;31:1163-1165.
 42. Kao CH, Lin WY, Wang SJ, et al. Visualization of suppressed thyroid tissue by Tc-99m MIBI. *Clin Nucl Med* 1991;16:812-814.
 43. Foldes I, Levay A, Stotz G. Comparative scanning of thyroid nodules with technetium-99m pertechnetate and technetium-99m methoxyisobutylisonitrile. *Eur J Nucl Med* 1993;20:330-333.
 44. Kao CH, Wang SJ, Liao SQ, et al. Quick diagnosis of hyperthyroidism with semiquantitative 30-minute technetium-99m-methoxy-isobutyl-isonitrile thyroid uptake. *J Nucl Med* 1993;34:71-74.